Available online at www.sciencedirect.com
ScienceDirect
Earth and Planetary Science Letters 252 (2006) 481–489
EPSL
www.elsevier.com/locate/epsl

# Stress-dependent power-law flow in the upper mantle following the 2002 Denali, Alaska, earthquake

Andrew M. Freed [a,*], Roland Bürgmann [b], Eric Calais [a], Jeff Freymueller [c]

[a] Department of Earth and Atmospheric Sciences, Purdue University, West Lafayette, Indiana, USA
[b] Department of Earth and Planetary Science, University of California Berkeley, Berkeley, California, USA
[c] Geophysical Institute, University of Alaska Fairbanks, Fairbanks, Alaska, USA

Received 27 March 2006; received in revised form 3 October 2006; accepted 4 October 2006
Available online 7 November 2006
Editor: R.D. van der Hilst

**Abstract**

Far-field continuous Global Positioning System (GPS) time-series data following the 2002 M7.9 Denali, Alaska earthquake imply that mantle viscoelastic rheology is stress-dependent. A linear viscous mantle cannot explain fast early displacement rates at the surface that rapidly decay with time, whereas a power-law rheology where strain rate is proportional to stress raised to the power of $3.5 \pm 0.5$ provides decay rates and spatial patterns in agreement with observations. This is consistent with laboratory measurements for hot, wet olivine, implying a hydrated mantle and a relatively thin (60-km-thick) lithosphere beneath south-central Alaska. These results suggest that the viscous strength of the lithosphere varies both spatially and temporally, and that effective viscosities inferred from different loading events or observational time-periods can differ by up to several orders of magnitude. Thus, the very conditions that enable the inference of rheologic strength–transient loading and unloading events–significantly alter the effective viscosity.


*Keywords:* postseismic; power-law; Denali; viscoelastic; rheology; earthquake

## 1. Introduction

After decades of research on how the Earth's lower crust and upper mantle deform, there is still no consensus on which layer contributes more to the strength of the lithosphere [1,2]. The debate becomes even more challenging given the possibility of a stress-dependent rheology at depth (e.g., [3]), implying significant temporal and spatial variations in viscous strength as stresses from short-term perturbations, such as earthquakes or glacier unloading, dissipate. Stress-dependent rheology could help explain orders-of-magnitude different inferences of viscosity that arise from various postseismic and postglacial analyses of surface deformations, even within similar tectonic provinces. Laboratory experiments [4,5] suggest that stress-dependent rheology would arise from the occurrence of dislocation creep as the primary mechanism of viscous deformation. Indeed, seismic anisotropy data [6] and similarities between microstructures observed in naturally and experimentally deformed rocks [7], provide evidence of dislocation creep in the upper mantle and lower crust, but no measurement of the stress-dependence of the flow. Currently, knowledge of the stress-dependence of viscoelastic flow comes primarily from laboratory experiments,

* Corresponding author.
*E-mail address:* freed@purdue.edu (A.M. Freed).

0012-821X/$ - see front matter © 2006 Elsevier B.V. All rights reserved.
doi:10.1016/j.epsl.2006.10.011

where relatively high strain rates and stresses applied to mm-sized samples are often 7 or more orders of magnitude greater than tectonic levels, leading to uncertainty in how well laboratory power-laws describe bulk rheology. Here, we use GPS observations of postseismic deformation following the 2002, M7.9 Denali, Alaska earthquake to directly infer the viscous strength of the upper mantle, finding a rheology consistent with a laboratory-derived, stress-dependent, power-law for hot, wet olivine.

An earthquake can be used as a large rock deformation experiment in which sudden stress changes induce viscous flow in warm, deep regions of the lower crust and upper mantle that lead to observable surface deformation. By matching observed and calculated displacements as a function of time, it is possible to determine the relationship between strain rate and stress during viscoelastic relaxation. Previously, this has been attempted using postseismic observations following the 1992 M7.3 Landers and 1999 M7.1 Hector Mine earthquakes that showed evidence for power-law flow in the upper mantle beneath the Mojave Desert [8]. But these results are possibly inconclusive because the analysis assumed that viscoelastic flow was the dominant mechanism contributing to postseismic observations, even though afterslip and poroelastic rebound likely contributed to observed surface displacements [9–12]. Pollitz [13] used a transient rheology (a Burgers body; [14–16]) to explain post-Denali observations without consideration of other mechanisms, possibly explaining a poor fit to many near-field GPS stations.

Previous analysis of cumulative displacements over a 2-yr time period following the Denali earthquake suggests that motions recorded at stations within 100 km of the rupture surface include contributions from viscoelastic relaxation, afterslip, and poroelastic rebound [17]. The same analysis shows that 70–80% of the observed displacements at stations beyond 100 km (defined here as far-field, Fig. 1) are caused by viscoelastic relaxation at depths greater than 60 km, and that neither poroelastic rebound nor stress driven afterslip on a down-dip extension of the Denali fault within the mantle can produce the observed far-field deformation pattern [17]. This is consistent with the lack of a distinguishable discontinuity in the seismic velocity structure associated with the Denali fault below 60 km depth [18] and the inference of thin (order 60 km) mechanical lithosphere in subduction zone backarcs [19]. Modeling of glacial isostatic adjustment resulting from post-Little Ice Age and recent glacier melting in southeast Alaska also supports this lithospheric thickness [20]. Thus, observed far-field

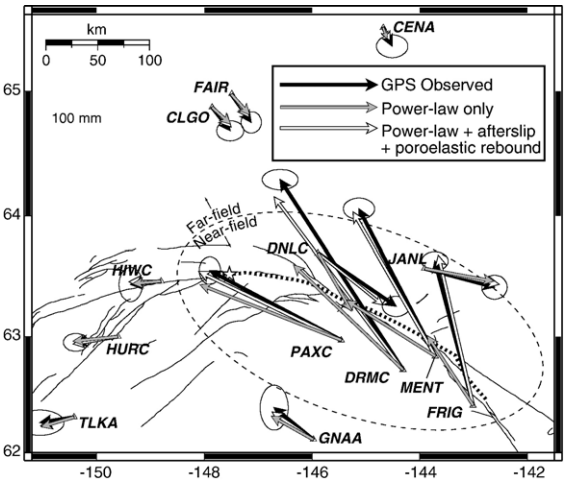


Fig. 1. Observed and calculated, cumulative surface displacements for the 3-yr period following the 2002 Denali earthquake. Only data at continuous GPS stations are shown, as these are the instruments that provide daily time-series required to sufficiently constrain displacement rate changes needed to infer the relationship between strain rate and stress during viscoelastic relaxation. GPS stations outside of the dashed oval are considered far-field stations where displacements are primarily (70–80%) due to flow below 60 km [17]. The power-law displacements are based on a power-law model with an exponent of $n=3.5$ and a depth dependent power-law parameter, $C$, in Fig. 4. The multiple mechanism model consists of the power-law rheology plus shallow afterslip and poroelastic rebound as described in [17]. The figure illustrates that power-law flow in the lower crust and upper mantle are sufficient to explain far-field displacements, while the addition of shallow afterslip and poroelastic rebound are required to explain near-field displacements.

displacements following the Denali earthquake provide a unique opportunity to resolve the rheology of the Alaskan uppermost mantle. Of the 20–30% contribution of deformation within the lower crust to far-field surface displacements, it is more difficult to isolate the relative influence of viscoelastic relaxation versus afterslip, in part because both mechanisms lead to similar deformation patterns [17]. However, as the present analysis focuses on mantle rheology, it is more important here to quantify the relative magnitude and rate of deformation within the lower crust than it is to fully understand the acting mechanism. We model postseismic deformation within the lower crust as being due to viscoelastic relaxation knowing that such a model may be serving as a proxy for afterslip.

## 2. Methods and data

Laboratory derived flow laws associated with dislocation creep suggest a power-law of the form:

$$\dot{\varepsilon} = A\ \sigma^n\ e^{(-Q/RT)} \quad \text{or} \quad \eta = \sigma^{(1-n)}\ e^{(Q/RT)}/2A \qquad (1)$$

where $\dot{\varepsilon}$ is strain rate ($s^{-1}$), $\eta$ is the effective viscosity (Pa s), $A$ is a pre-exponential factor ($MPa^{-n}$ $s^{-1}$), $\sigma$ is the differential stress (MPa), $n$ is the power-law exponent, $Q$ is the activation energy (kJ $mol^{-1}$), $R$ is the universal gas constant (J $mol^{-1}K^{-1}$), and $T$ is temperature (K) (e.g., [4]). As most of these parameters can be assumed constant during a single postseismic cycle, we can simplify the expressions for postseismic analysis to the form:

$$\dot{\varepsilon} = \sigma^n / 2C \quad \text{or} \quad \eta = C\,\sigma^{(1-n)} \tag{2}$$

where we define a power-law parameter, $C$ ($Pa^n$ s). This formulation reduces the number of variables to infer in a postseismic analysis to $n$ and $C$, though $C$ varies with

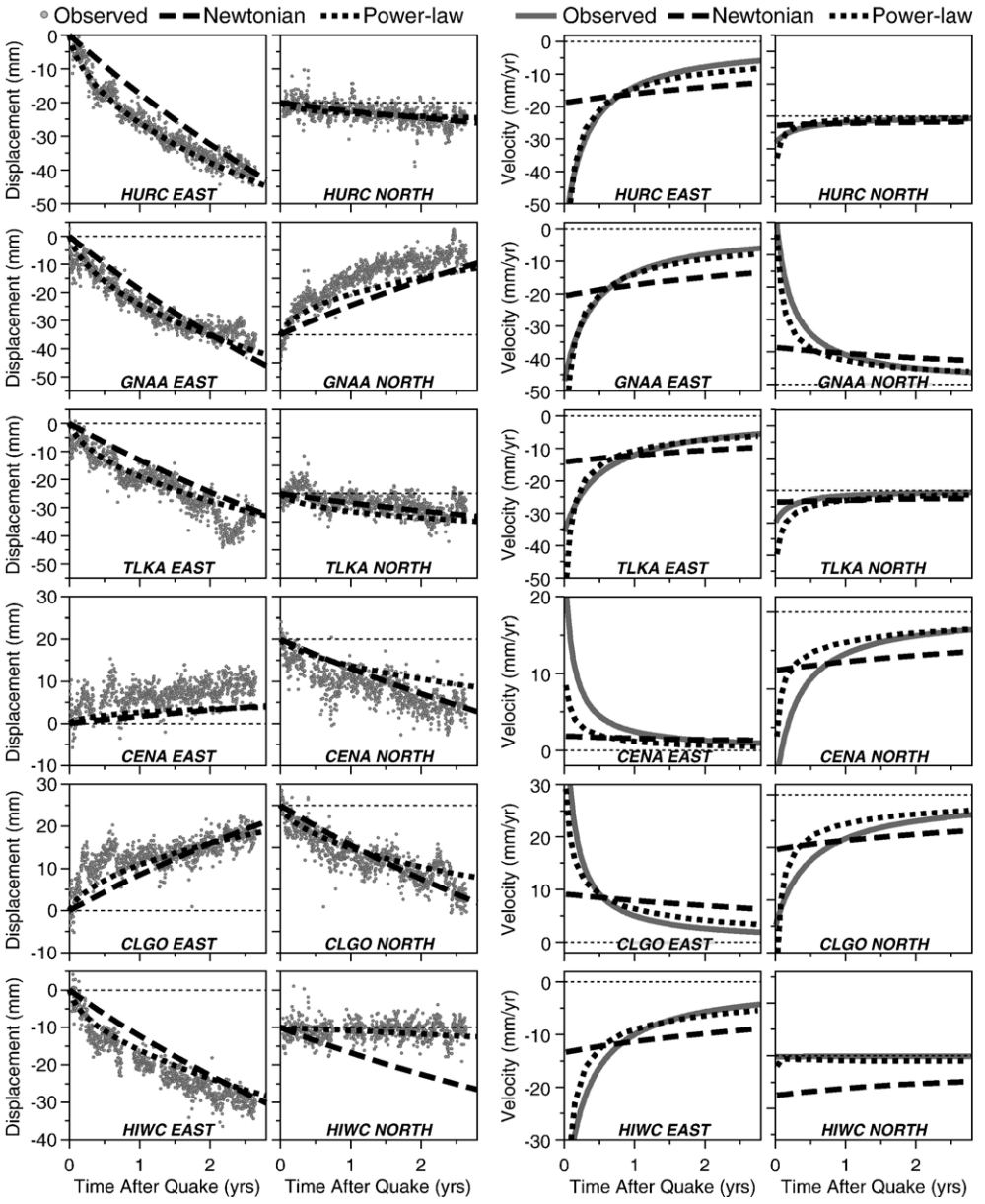


Fig. 2. Left columns: Comparison of observed GPS position time-series and displacements calculated by best-fit Newtonian ($n=1$) and power-law models ($n=3.5$) for far-field stations (Fig. 1). Time-series for station FAIR are used in model testing but not shown, as it mimics data of the nearby station CLGO. Annual, semi-annual, and secular components have been removed from the observed time-series [17]. Right columns: Comparison of GPS observed velocity (based on a logarithmic fit to the data) and that calculated by Newtonian and power-law models. Horizontal dashed lines indicate zero displacement/velocity.

depth. If $n=1$ (Newtonian rheology), these equations imply that viscosity is stress-invariant (equal to a depth-dependent $C$), and that strain rate increases linearly with stress. If $n>1$ – laboratory-derived power-law exponents for lower crustal and upper mantle rocks usually range from 2.5 to 4 [4] – these equations imply a decrease in effective viscosity and a significant increase of strain rate as differential stress increases. As coseismic stresses dissipate after an earthquake through the process of viscoelastic relaxation, reduced viscosities will recover to prequake levels, and strain rates will rapidly drop.

We use changes in the rate of observed surface motions, which reflect changes in the rate of viscoelastic flow at depth, to infer the power-law exponent of the rheology. This is accomplished by developing a finite element simulation of postseismic relaxation and determining the rheology of the lower crust and upper mantle that leads to the best fit to the position time-series at far-field GPS sites (Fig. 2) with the added constraint that candidate rheologies cannot lead to displacements and rates larger than observed at near-field stations (<100 km distance from rupture, Fig. 1). We utilize the same mesh, assumed prequake tectonic model, and coseismic slip distribution as in our earlier Newtonian study of cumulative displacement [17]. Knowledge of the pre-earthquake absolute state of stress is needed in stress-dependent rheology studies. For each candidate rheology we solve for the steady-state stress level that is in equilibrium with the regional strain rate, as determined from a tectonic block model fit to GPS data [21]. This is accomplished by applying velocity boundary conditions associated with block rotation to the south (see Fig. 4c in [17] for details), and allowing the system to evolve until stresses reach steady state levels in the lower crust and upper mantle. Coseismic slip is initiated after steady-state stress levels are reached (usually after ~400 yr). Steady-state stress levels are not achieved in the seismogenic portion of the crust, as this layer builds up elastic strain, but this layer does not participate in viscoelastic relaxation. Typical prequake differential stress levels are of the order of 1 MPa at 30 km depth, 0.1 MPa at 60 km depth, and 0.01 MPa at 100 km depth below the Denali fault. These stress levels will rise to the order of 3.0, 0.5, and 0.1 MPa at 30, 60, and 100 km depth, respectively, due to coseismic slip associated with the Denali earthquake. The modeled block rotation simulates the major component of shear acting on the Denali region, but

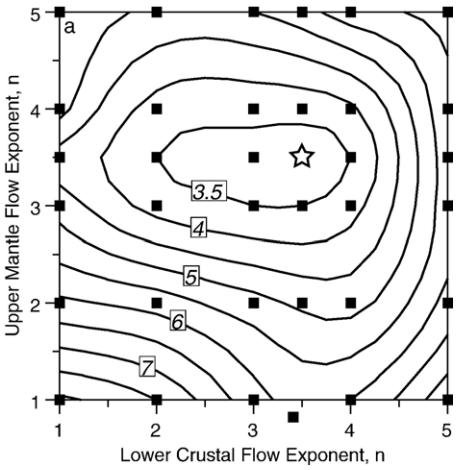


Fig. 3. Contours of rms misfit (0.5 mm increments) as a function of power-law exponent, $n$, assumed for lower crustal and upper mantle rheology, where rms=sqrt[$(1/m)\sum(d_o-d_c)^2$], $d_o$ and $d_c$ are the observed and calculated displacements and $m$ is the total number of observations. Misfit calculations use observations at 2 month increments based on a logarithmic fit of the time-series displacements. Squares show the stress exponents modeled. The depth-distribution of the power-law parameter $C$ (Eq. (2)) was optimized to minimize the misfit for each exponent model (see Fig. 4). A minimum misfit of 3.2 mm was found for a model where both the lower crust and upper mantle have power-law exponents of $n=3.5$ (star).

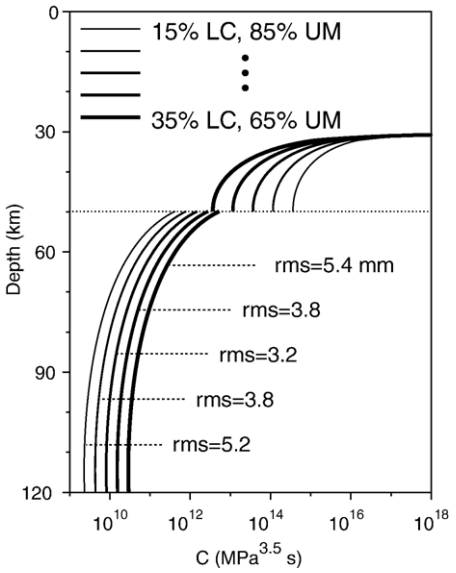


Fig. 4. Trade-offs between the relative strength of the lower crust (LC) and upper mantle (UM) for a model in which both layers are modeled with a power-law exponent of $n=3.5$. Strength is varied by shifting the relative magnitude of the power-law parameter $C$ within each region. The percentages shown in the legend are the resulting average contributions to far-field displacements from each region for the distribution of $C$ plotted. The best fitting (rms=3.2 mm) model has mantle flow contributing 75% of the far-field displacements and lower crustal flow contributing 25%.

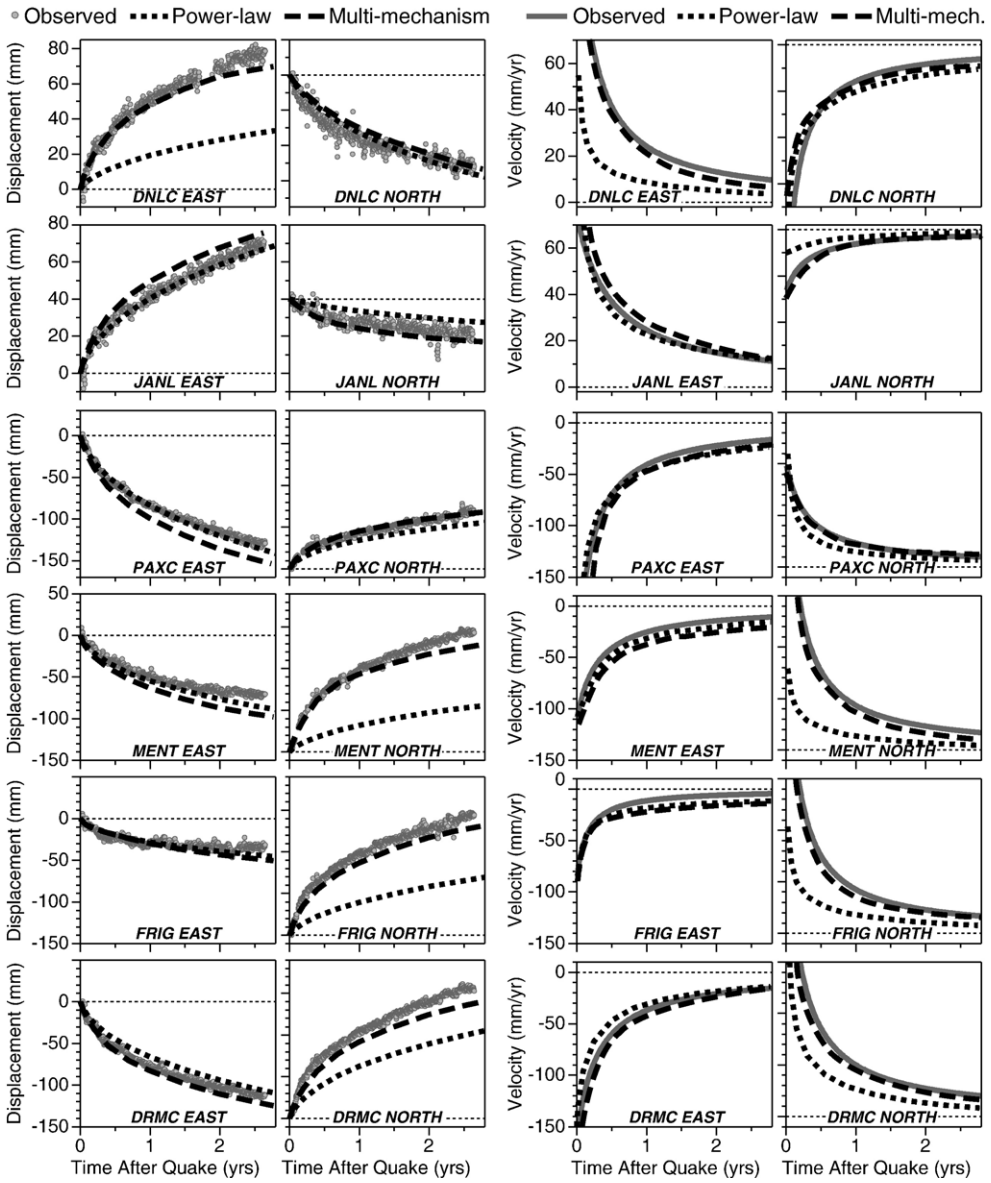


Fig. 5. Left columns: Comparison of observed GPS position time-series and displacements calculated by viscoelastic flow due to a power-law ($n$=3.5) rheology and due to a combination of power-law flow, shallow afterslip, and poroelastic rebound for near-field stations (Fig. 1). Annual, semi-annual, and secular components have been removed from the observed time-series [17]. Right columns: Comparison of GPS-observed velocity (based on a logarithmic fit to the data) and that predicted by power-law only and by the combination model. Horizontal dashed lines indicate zero displacement/velocity.

does not take into account loading due to subduction of the Pacific plate and collision of the Yakutat block to the south. We experimented with applying boundary conditions to the south that led to compression of the region and with variations on the rate of block rotation to gage the impact of errors in the prequake stress field on our conclusions. We found that variations in the absolute stress field could be compensated for by modifying the strength parameter $C$ in Eq. (2), but did not significantly change the inferred power-law exponent, $n$.

It should also be noted that we did not attempt to match prequake (interseismic) velocities with each candidate viscoelastic rheology. We inferred prequake velocities from a deep slip model as described in [17]. Thus, we have not attempted to meet the sensible constraint laid out by Hetland and Hager [22] that a single consistent rheology should be found to explain

Table 1
Summary of laboratory parameters used in thermal calculations for Fig. 3c

| | Composition | Pre-exponential factor, A ($MPa^{-n}s^{-1}$) | Power-law exponent, $n$ | Activation energy, Q ($KJ\ mol^{-1}$) | Ref. |
|---|---|---|---|---|---|
| Lower crust | Dry Columbia | 8.0 | 4.7 | 485 | [23] |
| Lower crust | Wet anorthite | 2.6 | 3.0 | 356 | [24] |
| Upper mantle | Wet olivine | $4.89\times10^{6}$ | 3.5 | 515 | [25] |
| Upper mantle | Dry olivine | $4.85\times10^{4}$ | 3.5 | 535 | [25] |

both postseismic and interseismic observations. This important constraint was beyond the scope of the present modeling and will be considered in a future study.

## 3. Results

In order to determine the rheology of the lower crust and upper mantle that best matches displacement and velocity time-series at far-field sites, we considered power-law exponents from 1 to 5, allowing for different exponents to characterize the lower crust and the upper mantle. In each case we iteratively solved for the best-fitting depth dependence of the power-law parameter $C$, with the assumption that $C$ decreases with depth within the lower crust and, separately, within the upper mantle, owing to increasing temperature. We assume no other functional form and do not consider lateral variations of $C$. We explored models in which the decrease in C with depth was insignificant and models where $C$ decreases by several orders of magnitude. We found that a power-law exponent of $n=3.5\pm0.5$ in the upper mantle, combined with a power-law exponent of $n=3\pm1$ in the lower crust, provide the best fit to observed surface displacements and velocities (Fig. 3). An optimized Newtonian ($n=1$) rheology led to almost three times the misfit of a model that assumes a power-law exponent of $n=3.5$. This result can be visualized by comparing observed displacement and velocity time-series to those calculated for these respective rheologies (Fig. 2). The best-fit Newtonian rheology underpredicts early, fast rates of displacement, then overpredicts rates in the years following the quake. This is most clearly seen in the comparison to velocity time-series. In contrast, a power-law rheology of $n=3.5$ (dotted lines in Fig. 2) correctly predicts the trends observed on most displacement and velocity time-series.

Though the Denali far-field displacements require flow primarily in the mantle, there are limited trade-offs between lower crustal and upper mantle contributions. Fig. 4 shows a series of $n=3.5$ models in which the relative strength (as denoted by the value of $C$) of the lower crust and upper mantle are varied. From the best-fitting model, values of $C$ for the lower crust can be decreased (more flow) by ~20% in association with an increase in the values of C of ~10% for the upper mantle without significantly increasing the misfit. This corresponds to the lower crust contributing a maximum of ~30% to the far-field displacements, compared to ~20% for the model in which lower crust flow is minimized.

The viscoelastic power-law model works well to explain cumulative far-field displacements (Fig. 1) and far-field time-series (Fig. 2). However, this model underpredicts many of the near-field observations of cumulative displacement (Fig. 1) and near-field time-series (Fig. 5). The underprediction of near-field displacements demonstrates the need to consider other active postseismic mechanisms. We can explain the near-field time-series as well by considering the influence of shallow afterslip and poroelastic rebound as inferred in our previous study [17]. Fig. 5 shows time-series of displacements and velocities observed at the six near-field stations (Fig. 1), those predicted by only power-law relaxation, and those predicted by a multi-mechanism model that includes power-law flow, shallow afterslip, and poroelastic rebound. The distribution of shallow afterslip was shown in Fig. 13b of Freed et al. [17]. The afterslip contribution is assumed to decay following a logarithmic function with a decay time-constant of 0.1 yr, while the poroelastic rebound component is assumed to linearly decay to zero at 6 months. Because they are shallow sources, the contributions of afterslip and poroelastic rebound enable a good fit to near-field data, while not significantly influencing far-field displacements (Fig. 1).

## 4. Discussion and conclusions

To understand how the strength of the lithosphere beneath the Denali fault inferred from postseismic surface deformations compares to laboratory flow laws, we can combine Eqs. (1) and (2) into

$$T = Q/R\ \ln(2AC) \tag{3}$$

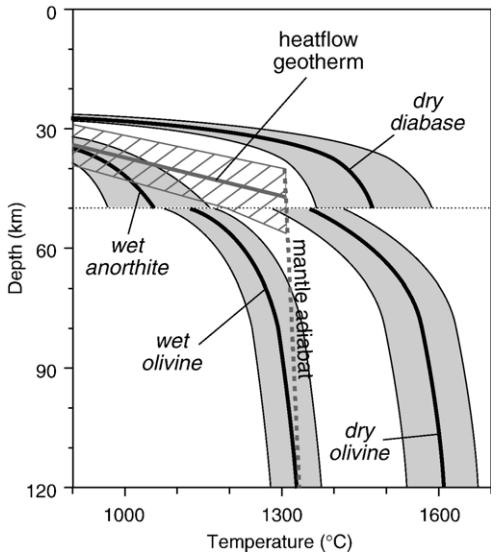


Fig. 6. Calculated geotherms (from Eq. (3)) based on laboratory power-law parameters of wet and dry lower crustal and upper mantle materials (Table 1) and the best fitting postseismic models from this study are shown as bold curves. Grey regions around these geotherms represent the uncertainty with regard to trade-offs between the upper mantle and lower crustal flow. A geotherm calculated based on a surface heatflow of 75±15 mW/m$^2$ in backarcs is shown as a grey line with hachured region, and the onset of a mantle adiabat is shown as a dashed grey line [19].

and solve for temperature as a function of the depth-dependent parameter $C$ (inferred from this study) and the laboratory derived parameters $A$ and $Q$ for a given sample material. The equation above, which assumes the same $n$ in postseismic calculations and laboratory experiments, can be used to calculate an inferred geotherm for the postseismically deforming portion of the Alaskan lithosphere. This calculation assumes that temperature is the only factor influencing variations of $C$ with depth. This is a reasonable first-order assumption, although water fugacity (and other factors) may also vary with depth. We considered several possible compositions for the lower crust and upper mantle (Table 1). Fig. 6 shows four calculated geotherms (bold curves) based on laboratory derived power-law parameters for these compositions, and the best-fitting $C$.

Well-temperature gradients in south-central Alaska suggest heat flow in the 75±15 mW/m$^2$ range [26], which is consistent with a compilation of heat flow observations of non-extending backarcs worldwide [19]. This region is only partially in an active backarc setting, but has been in a subduction or collisional setting for at least tens of millions of years, so that a similar geotherm is expected. Currie and Hyndman [19] have calculated theoretical geotherms for backarcs or recent backarcs based on this heat flow range (grey region in Fig. 3c) and Ito and Katsura [27] have derived a mantle adiabat from laboratory experiments. The estimated adiabat is consistent with thermal models derived from seismic velocities to the west of the Denali rupture zone, which suggest that temperatures can get as high as 1400 °C at 100 km depth [28].

Fig. 6 shows that the inferred mantle geotherm produced by assuming a wet-olivine rheology compares well with that estimated from heat flow and the adiabat, consistent with the presence of water due to slab dehydration [29]. The model-derived geotherm assuming a dry olivine mantle requires ~1600 °C mantle temperatures, which represents a compensation for an assumed rheology that is much too strong. The weak hydrated mantle we infer at relatively shallow depths (60 km) beneath southern Alaska is consistent with studies that require the presence of shallow convection to explain

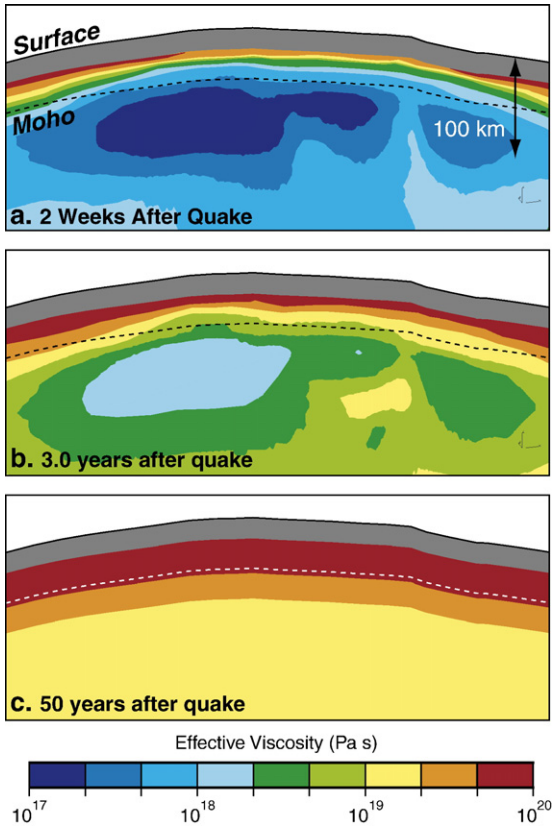


Fig. 7. Calculated effective viscosity along a cross-section through the Denali fault as a function of time with respect to the Denali earthquake: (a) 2 weeks after the earthquake, (b) 3 yr after the earthquake, (c) 50 yr or long-term steady state (also prequake). The calculation of effective viscosity is not accurate for the upper 25 km of the crust (grey region), where steady-state prequake stresses could not be calculated. Thus, viscosities are not shown for this region.

high heat flow in backarc regions [30,31]. In the crust, an assumption of wet anorthite is found to be consistent with temperatures estimated from heat flow. While an assumption of dry diabase appears too strong (inferred temperatures too high), such a rheology could be realistic if a significant portion of postseismic flow in the lower crust was accommodated by a weak shear zone as opposed to viscoelastic relaxation.

One of the broader implications of a stress-dependent rheology is the effective viscosity variation as a function of time in response to different magnitude earthquakes (and other loading/unloading processes). In the present analysis, we infer an effective viscosity of $\sim 10^{17}$ Pa s confined to a volume beneath the fault for the first 2 weeks after the earthquake (Fig. 7a). The viscosity of this region of the mantle rapidly increases to $\sim 2\times 10^{18}$ Pa s 3 yr later (Fig. 7b). Eventually, after about 50 yr the viscosity of this region will recover most of the way back to prequake levels of $\sim 2\times 10^{19}$ Pa s (Fig. 7c). This interseismic viscosity is consistent with other studies of long-term mantle wedge viscosity [32–35]. Thus, the rheologic strength of the upper mantle beneath the Denali quake cannot be described by a single viscosity structure in time or space. In addition, the volume in which low viscosity is concentrated in the first few weeks after the earthquake represents a focused region of deformation where postseismic strains are localized. For Newtonian models, where the viscosity is laterally homogenous, postseismic strains are more diffuse, spreading over a region that is more than three times that of the power-law rheology. Thus, power-law rheology serves to focus high postseismic strain rates under faults early on, a characteristic that may play an important role in the perseverance of major faults. Additional weakening mechanisms (e.g., by grain size reduction, mineral reactions or shear heating) may further localize deformation in the lower crust.

The variability of viscosity associated with power-law flow has direct bearing on the current debate on lithospheric strength. For some, the lithosphere is best described by a rheology in which a weak lower crust is sandwiched between a strong upper crust and a strong upper mantle (so-called "jelly sandwich" model (e.g., [36])). For others the lithosphere has a weak mantle and its strength resides mostly in the upper crust [so-called "crème brûlée" model (e.g., [2])). Our results suggest that immediately after an earthquake or other transient loading event, the upper mantle in south-central Alaska behaves as a relatively weak region, concentrating strength in the upper and middle crust. This finding is consistent with a crème brûlée model, which may be appropriate for much of western North America [31]. In the long-term, and at some distance from active faults, the lower stress environment associated with steady plate motions leads to an upper mantle with significantly greater strength, though not to the level of the upper and middle crust. Thus, in a hot, wet backarc or former backarc setting, a jelly sandwich characterization may never apply. However, in a cooler, dryer environment, such as that found in the interior of most tectonic plates (e.g., [29]), the mantle would likely provide significant strength to preserve the integrity of tectonic plates in a lower stress environment. Depending on the relative strength of the lower crust in continental interiors, a jelly sandwich model may then be an appropriate representation. Even in plate interiors a stress-dependent mantle rheology would still lead to a temporarily weakened mantle in response to significant transient loading, such as due to glacial rebound or a large intraplate earthquake. Thus, the characterization of lithospheric strength strongly depends on the loading environment.

## Acknowledgments

We thank Roy Hyndman, Claire Currie, and Peter Van Keken for helpful discussions regarding subduction zone lithospheric and thermal structure. We also thank Eric Hetland for his insightful review that helped us improve the clarity of the manuscript. This project is funded by NSF EAR grants 0309620-EAR and SGER-0312427-EAR to Purdue, EAR-0310410 and EAR-0328043 to UAF, and EAR-0309946 to UCB.

## References

[1] J. Jackson, Strength of the continental lithosphere: time to abandon the jelly sandwich? GSA Today 12 (2002) 4–10, doi:10.1130/1052-5173(2002)012<0004:SOTCLT>2.0.CO;2.
[2] E.B. Burov, A.B. Watts, The long-term strength of continental lithosphere: "jelly sandwich" or "crème brûlée"? GSA Today 16 (2006), doi:10.1130/1052-5173(2006)016.
[3] D. Kohlstedt, B. Evans, S. Mackwell, Strength of the lithosphere: constraints imposed by laboratory experiments, J. Geophys. Res. 100 (1995) 17587–17602.
[4] S.H. Kirby, A.K. Kronenberg, Rheology of the lithosphere; selected topics, Rev. Geophys. 25 (1987) 1219–1244.
[5] N.L. Carter, M.C. Tsenn, Flow properties of continental lithosphere, Tectonophysics 136 (1987) 27–63.
[6] P. Silver, D. Mainprice, W.B. Ismail, A. Tommasi, Mantle structural geology from seismic anisotropy, Mantle Petrology: Field Observations and High Pressure Experimentation: a Tribute to Francis R. (Joe) Boyd, Geochemical Society, Spec. Publ., vol. 6, 1999, pp. 79–103.
[7] G. Hirth, C. Teyssier, W.J. Dunlap, An evaluation of quartzite flow laws based on comparisons between experimentally and naturally deformed rocks, Int. J. Earth Sci. 90 (2001) 77–87.
[8] A.M. Freed, R. Bürgmann, Evidence of power-law flow in the Mojave Desert mantle, Nature 430 (2004) 548–551.

[9] G. Peltzer, P. Rosen, F. Rogez, K. Hudnut, Poroelastic rebound along the Landers 1992 earthquake surface rupture, J. Geophys. Res. 103 (1998) 30131–30145.
[10] T. Masterlark, H.F. Wang, Transient stress-coupling between the 1992 Landers and 1999 Hector Mine, California, earthquakes, Bull. Seismol. Soc. Am. 92 (2002) 1470–1486.
[11] J.C. Savage, J.L. Svarc, W.H. Prescott, Near-field postseismic deformation associated with the 1992 Landers and 1999 Hector Mine, California, earthquakes, J. Geophys. Res. 108 (2003), doi:10.1029/2002JB002330.
[12] Y. Fialko, Evidence of fluid-filled upper crust from observations of postseismic deformation due to the 1992 M(w)7.3 Landers earthquake, J. Geophys. Res. 109 (2004), doi:10.1029/2004JB002985.
[13] F.F. Pollitz, Transient rheology of the upper mantle beneath central Alaska inferred from the crustal velocity field following the 2002 Denali earthquake, J. Geophys. Res. 110 (2005), doi:10.1029/2005JB003672.
[14] W. Peltier, P. Wu, D. Yuen, The viscosities of the earths mantle, anelasticity in the Earth, in: F.D. Stacey, A. Nicolas, M.S. Peterson (Eds.), American Geophysical Union Geodynamics Series, AGU (American Geophysical Union), Washington, DC, 1981, pp. 59–71.
[15] Carter, Ave'Lallement, High temperature flow of dunite and peridotite, Geol. Soc. Amer. Bull. 81 (1970) 2181–2202.
[16] Chopra, High-temperature transient creep in olivine rocks, Tectonophysics 279 (1997) 93–111.
[17] A.M. Freed, R. Bürgmann, E. Calais, J. Freymueller, S. Hreinsdóttir, Implications of deformation following the 2002 Denali, Alaska earthquake for postseismic relaxation processes and lithospheric rheology, J. Geophys. Res. 111 (2006), doi:10.1029/2005JB003894.
[18] D. Eberhart-Phillips, D.H. Christensen, T.M. Brocher, R. Hansen, N.A. Ruppert, P.J. Haeussler, G.A. Abers, Imaging the transition from Aleutian subduction to Yakutat collision in central Alaska, with local earthquakes and active source data, J. Geophys. Res. (in press).
[19] C.A. Currie, R.D. Hyndman, The thermal structure of subduction zone backarcs, J. Geophys. Res. 111 (2006) B08404, doi:10.1029/2005JB004024.
[20] C.F. Larsen, R.J. Motyka, J.T. Freymueller, K.A. Echelmeyer, E.R. Ivins, Rapid viscoelastic uplift in southeast Alaska caused by post-Little Ice Age glacial retreat, Earth Planet. Sci. Lett. 237 (2005) 548–560.
[21] H.J. Fletcher, Crustal deformation in Alaska measured using the Global Positioning System, University of Alaska Fairbanks, Ph. D. Thesis, University of Alaska Fairbanks (2002) 135 pp.
[22] E.A. Hetland, B.H. Hager, Postseismic and interseismic displacements near a strike–slip fault: a two-dimensional theory for general linear viscoelastic rheologies, J. Geophys. Res. 110 (2005), doi:10.1029/2005JB003689.
[23] S.J. Mackwell, M.E. Zimmerman, D.L. Kohlstedt, High-temperature deformation of dry diabase with application to tectonics on Venus, J. Geophys. Res. 103 (1998) 975–984.
[24] E. Rybacki, G. Dresen, Dislocation and diffusion creep of synthetic anorthite aggregates, J. Geophys. Res. 105 (2000) 26,017–26,036.
[25] G. Hirth, D.L. Kohlstedt, An evaluation of quartzite flow laws based on comparisons between experimentally and naturally deformed rocks, Int. J. Earth Sci. 90 (2001) 77–87.
[26] AAPG heatflow map, www.smu.edu/geothermal/heatflow/heatflow.htm.
[27] E. Ito, T. Katsura, A temperature profile of the mantle transition zone, Geophys. Res. Lett. 16 (1989) 425–428.
[28] G.A. Abers, P.E. van Keken, E.A. Kneller, A. Ferris, J.C. Stachnik, The thermal structure of subduction zones constrained by seismic imaging: implications for slab dehydration and wedge flow, Earth Planet. Sci. Lett. 241 (2006) 387–397.
[29] J.E. Dixon, T.H. Dixon, D.R. Bell, R. Malservisi, Lateral variation in upper mantle viscosity: role of water, Earth Planet. Sci. Lett. 222 (2004) 451–467.
[30] S. Honda, M. Saito, Small-scale convection under the back-arc occurring in the low viscosity wedge, Earth Planet. Sci. Lett. 216 (2003) 703–715.
[31] R.D. Hyndman, C.A. Currie, S.P. Mazzotti, Subduction zone backarcs, mobile belts, and orogenic heat, GSA Today 15 (2005), doi:10.1130/1052-5173.
[32] M.I. Billen, M. Gurnis, A low viscosity wedge in subduction zones, Earth Planet. Sci. Lett. 193 (2001) 227–236.
[33] G. Khazaradze, K. Wang, J. Klotz, Y. Hu, J. He, Prolonged postseismic deformation of the 1960 great Chile earthquake and implications for mantle rheology, Geophys. Res. Lett. 22 (2002), doi:10.1029/2002GL015986.
[34] H. Ueda, M. Ohtake, H. Sato, Postseismic crustal deformation following the 1993 Hokkaido Nansei-oki earthquake, northern Japan: evidence for a low-viscosity zone in the uppermost mantle, J. Geophys. Res. 108 (2003), doi:10.1029/2002JB002067.
[35] Y. Hu, K. Wang, J. He, J. Klotz, G. Khazaradze, Three-dimensional viscoelastic finite element model for postseismic deformation of the great 1960 Chilean earthquake, J. Geophys. Res. 109 (2004), doi:10.1029/2004JB003163.
[36] W.-P. Chen, P. Molnar, Focal depths of intracontinental and intraplate earthquakes and their implications for the thermal and mechanical properties of the lithosphere, J. Geophys. Res. 88 (1983) 4183–4214.